nature research

https://doi.org/10.1038/s41586-020-2809-4

Supplementary information

Seismic evidence for partial melt below tectonic plates

In the format provided by the authors and unedited

Symbol	*Description*	*Value*	*Units*
α	exponent	0.26	
A	prefactor	7.5×10^{2}	$s^{-\alpha}\mu m^{\alpha}$
d	grain size	1-100	mm
T_0	period	100	s
E	activation energy	424	kJ mol^{-1}
V	activation volume	6×10^{-6}	m^3 mol^{-1}

Table S1: Reference parameters for Eq. 1 after Jackson et al.[13]

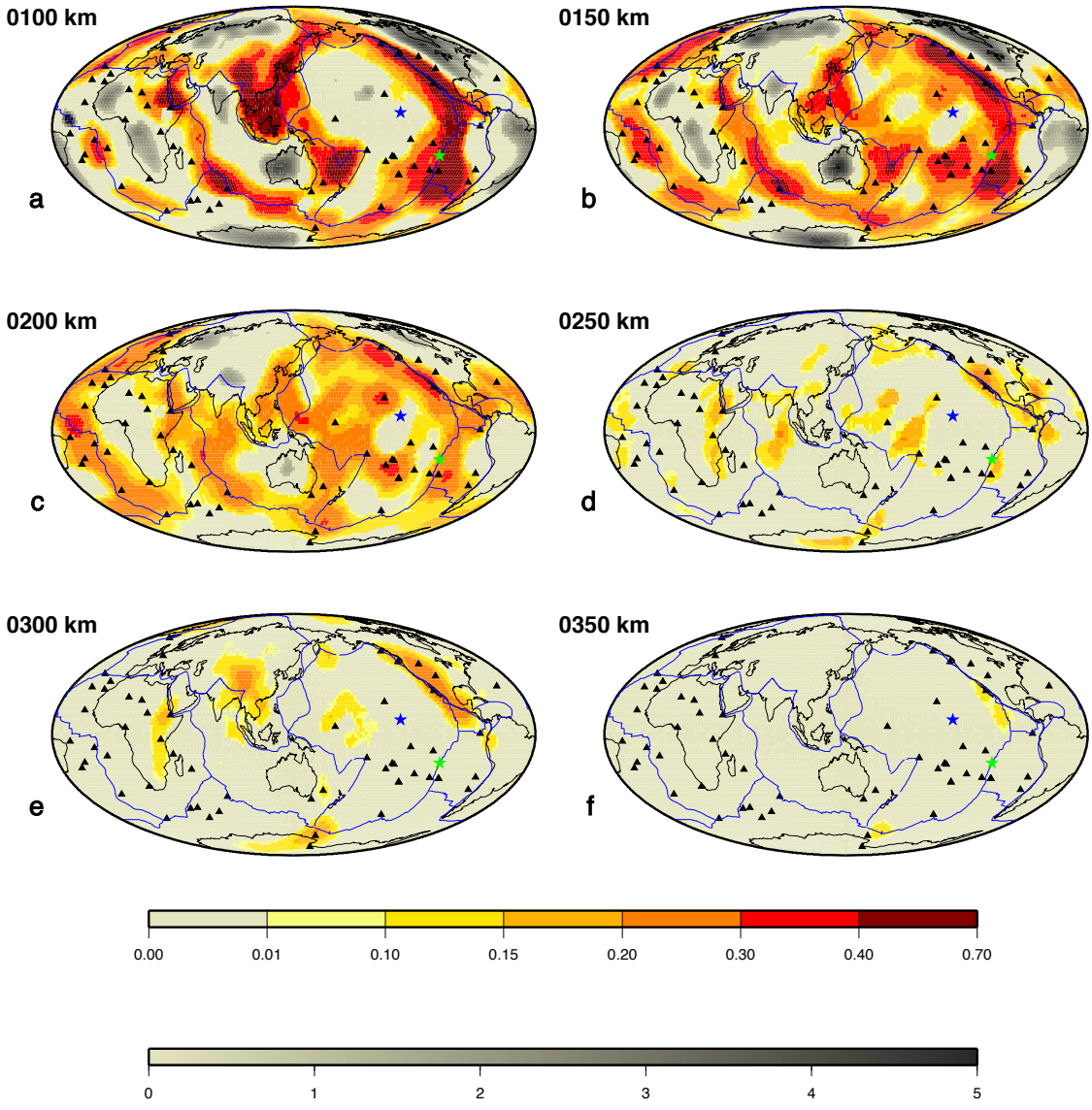

Fig. S1: Melt content at different depths assuming a 3D radial anisotropy model. Same as Figure 3 except that the isotropic 3D Vs model is based on our Sv observations corrected with the anisotropic ξ parameter of SEMUM2[38] (shown in Figure S2) instead of PREM. Melt content in percent is indicated with warm colours from ivory (0%) to brown (0.4 to 0.7%). The grey scale indicates the Vs misfit in percent between the theory and observations, in regions where Vs is too high compared with predictions.

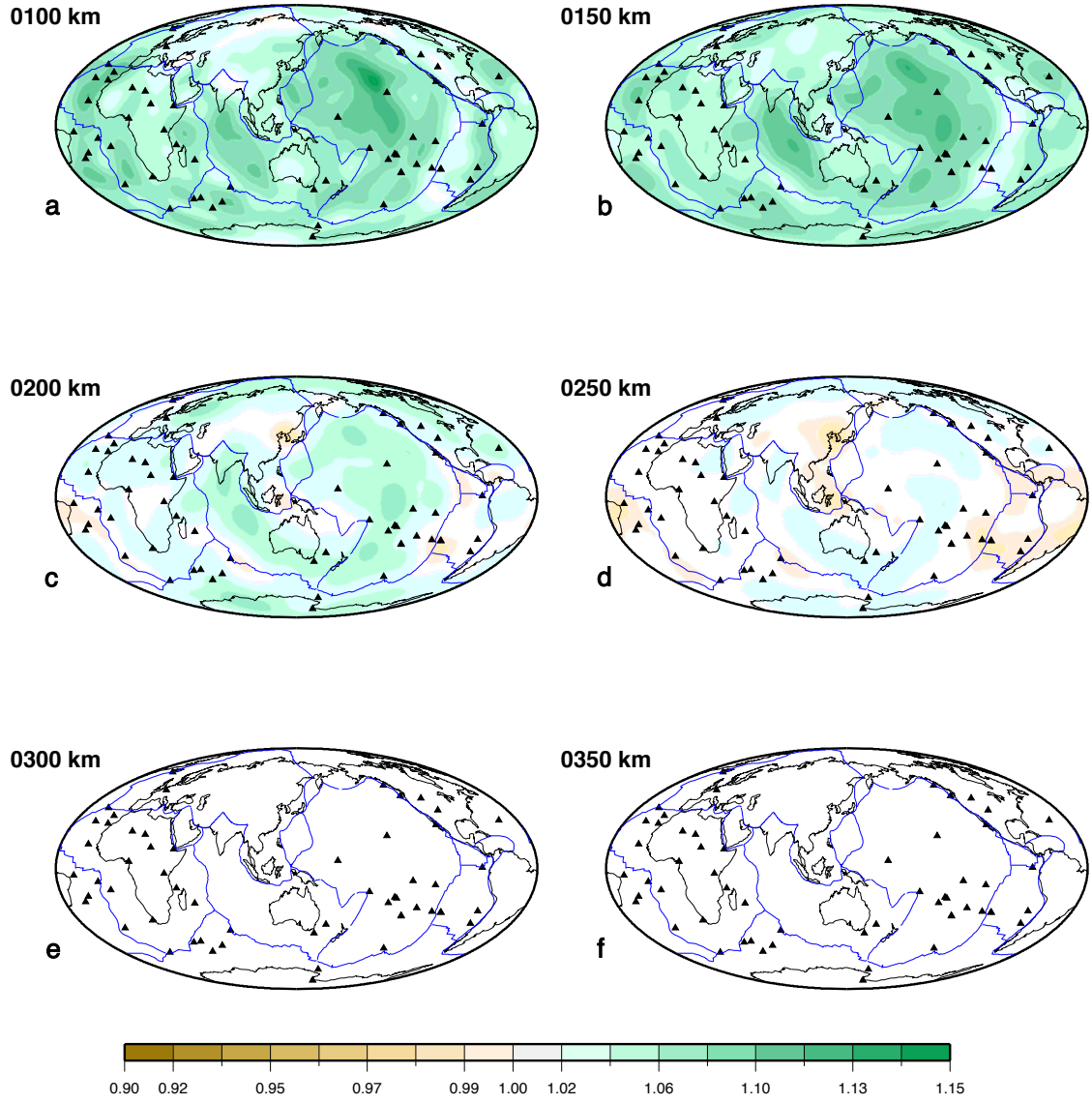

Fig. S2: Radial anisotropy maps at different depths in the upper mantle according to the SEMUM2[38] model. Radial anisotropy is displayed with the $\xi=(Vsh/Vsv)^2$ parameter.

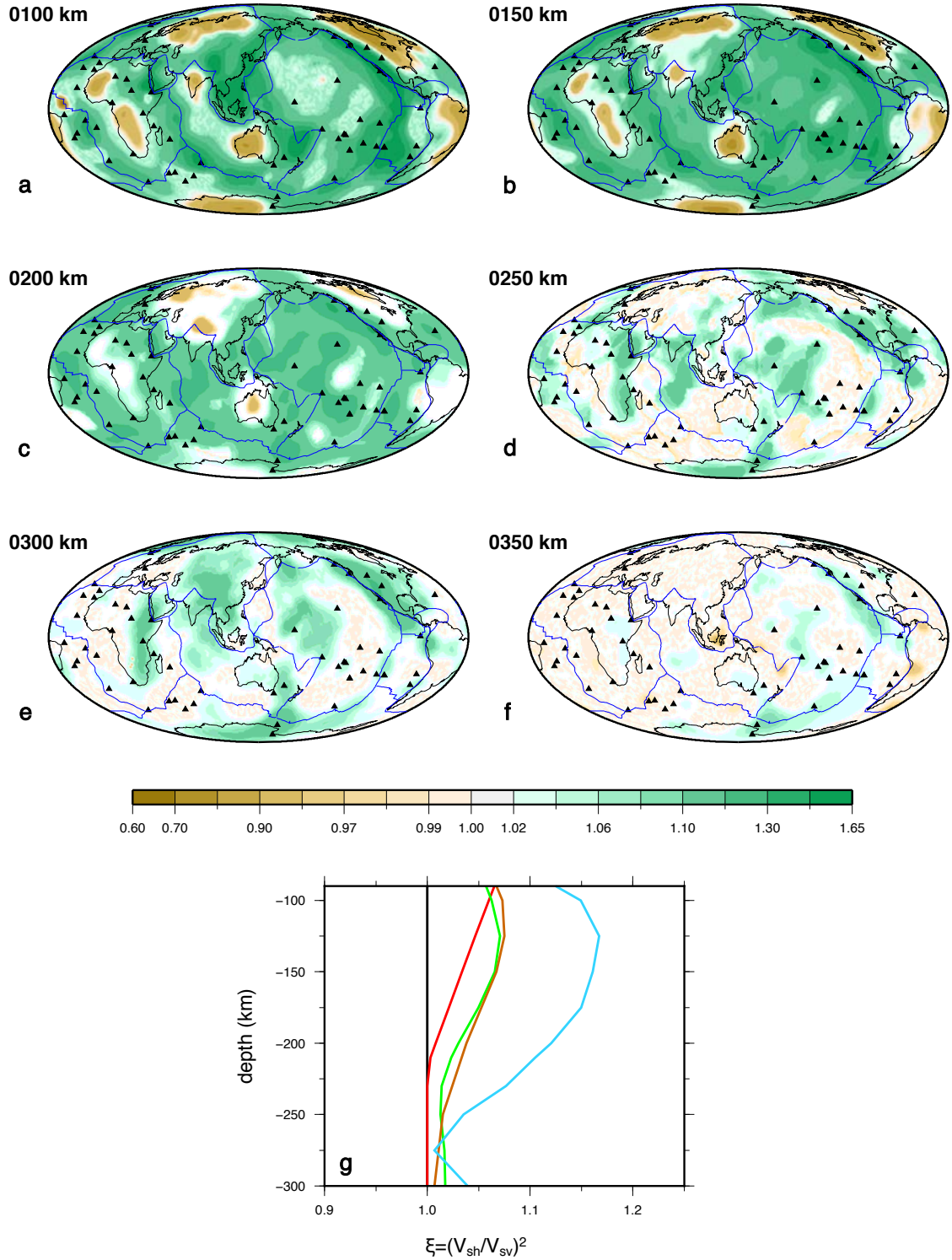

Fig. S3: Radial anisotropy needed to account for seismic observations without invoking mantle depletion or partial melt. Panels a-f: radial anisotropy maps (displayed with $\xi=(Vsh/Vsv)^2$) obtained by attributing the difference between our observed Vsv and the isotropic theoretical Vs to laterally varying Vsh rather than melt. The ξ values reach 1.65 and are much larger than the commonly observed values (<1.10, see Figure S2) especially in the oceanic asthenosphere. Panel g: global average of the required ξ (light blue curve) compared with the ξ of PREM (red curve) and the global averages of SEMUM2[38] (green curve) and S362ANI[39] (brown curve).

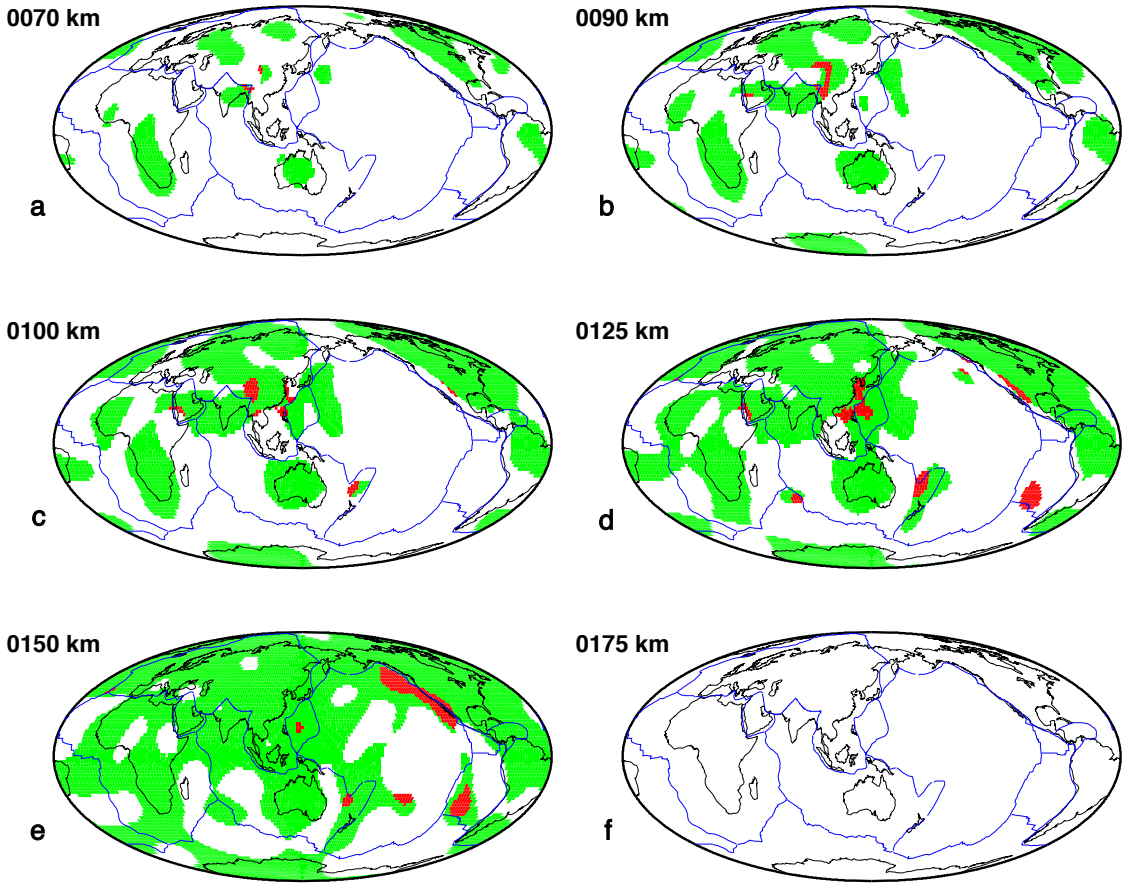

Fig. S4: Test of the elastically accommodated grain boundary sliding (EAGBS) hypothesis. Maps at different depths displaying in green the areas where conditions are favourable for EAGBS to be activated (see Methods). The red areas correspond to regions where EAGBS can reconcile our Qs and Vs observations. Grain size is 5 mm, following Karato et al.[40].

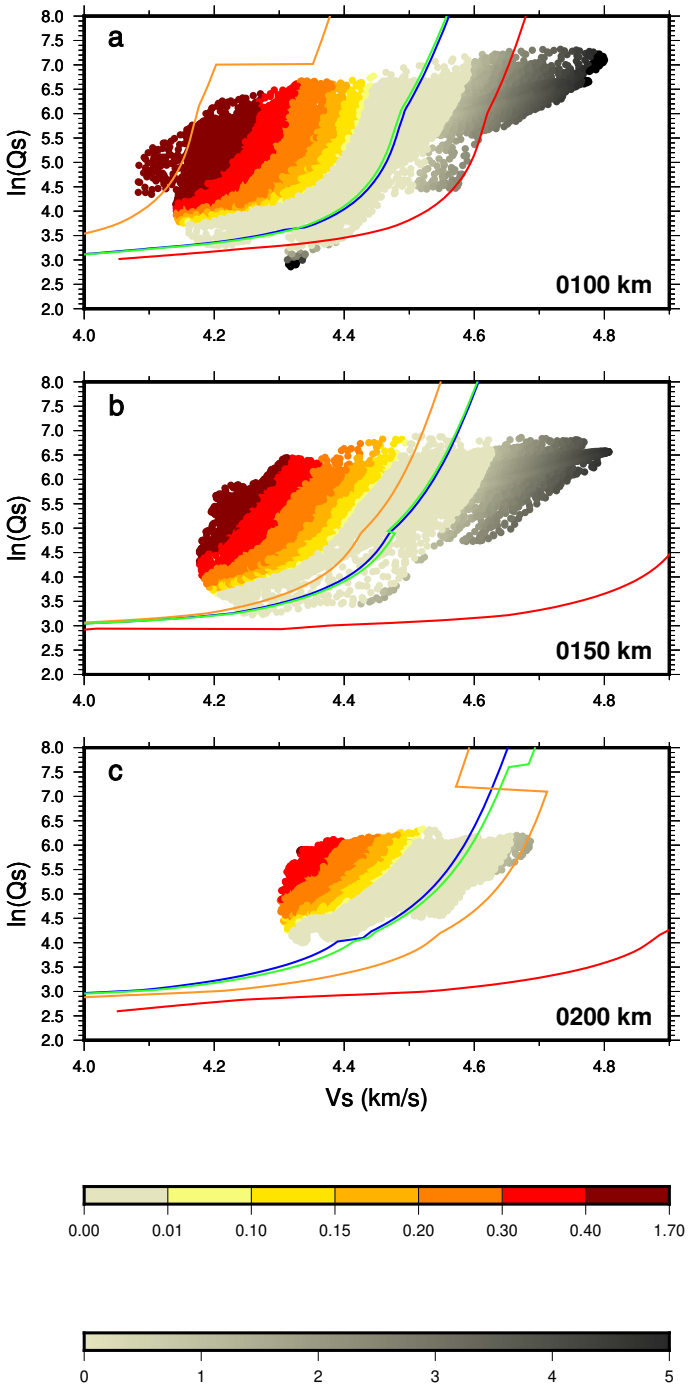

Fig. S5: Scatter plot showing shear attenuation as a function of shear velocity with theoretical curves for different compositions. Same as Figure 2 except that the green, orange and red theoretical curves correspond to harzburgite[44], silica-excess[16] and silica-deficient pyroxenite[44] compositions, respectively. The dark blue curve corresponds to the pyrolite[16] composition as in Figure 2. All curves are theoretical predictions in the case of no melt using the anelasticity model of Takei[4]. The colour scale indicates the amount of melt in percent required to explain our observations from the pyrolite composition (ivory colour from 0 to 0.01% of melt underlines data for which the model can reconcile our Qs and Vs observations). The grey scale indicates the Vs misfit in percent between theory and observations, in regions where Vs is too high and cannot be reconciled with model predictions.

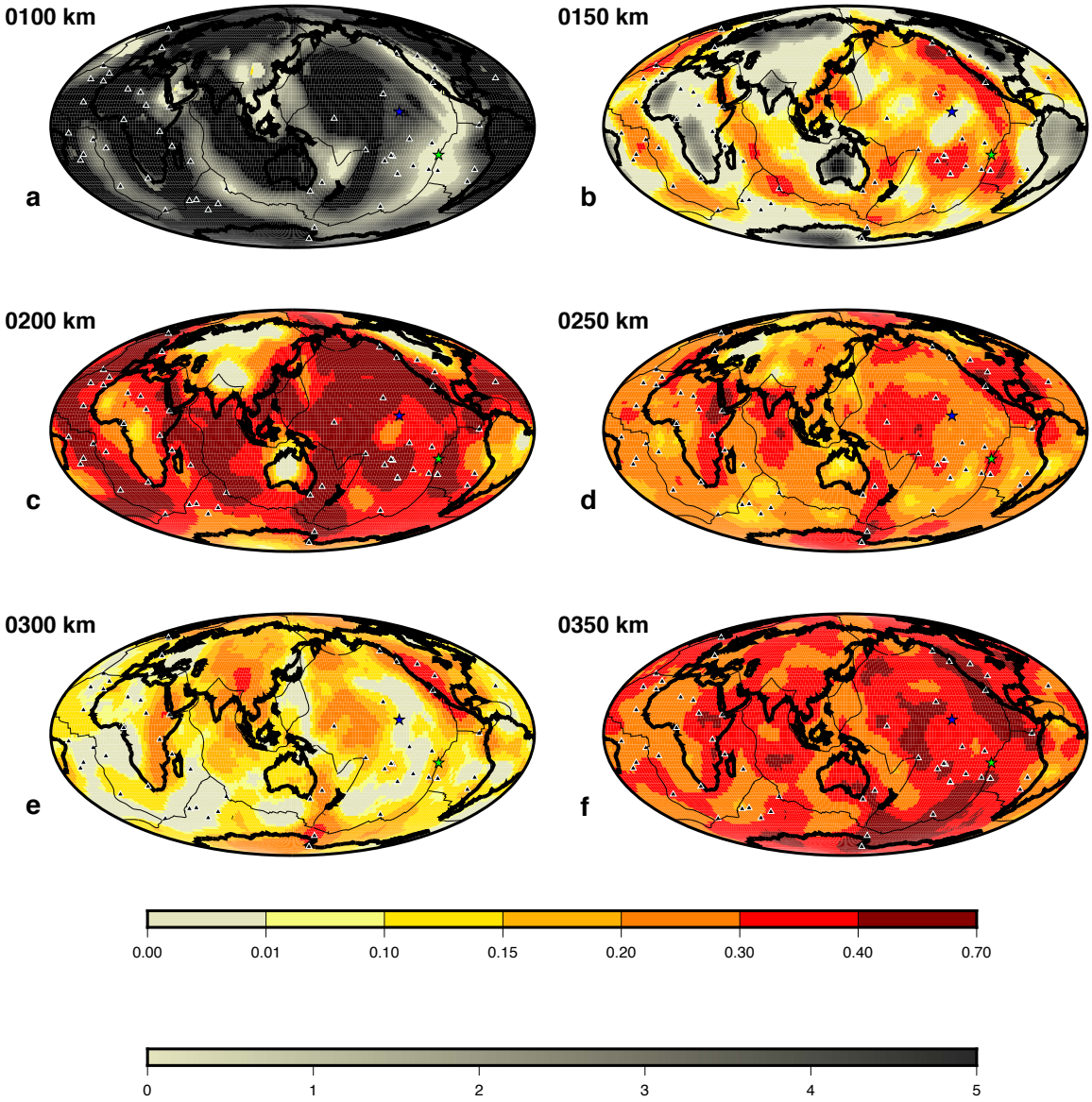

Fig. S6: Melt content at different depths in the upper mantle, assuming a basaltic composition (or silica-excess pyroxenite). The composition is taken from Table 1 of Xu et al.[16]. Maps are derived from the joint interpretation of QsADR17 and DR2020s.

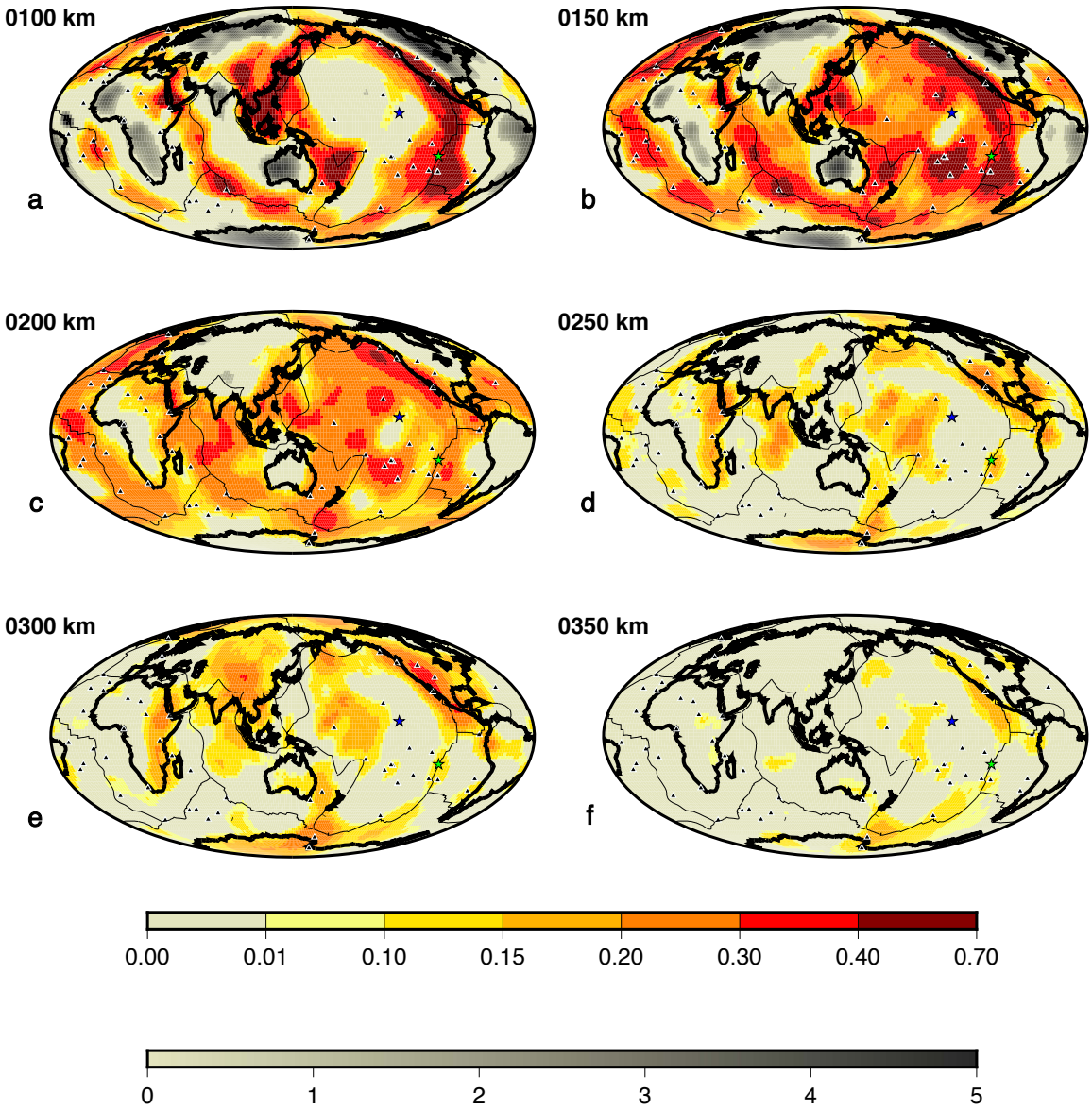

Fig. S7: Melt content at different depths in the upper mantle derived from the joint interpretation of QsADR17 and DR2020s, assuming a harzburgite composition. The composition is taken from Table 1 of Stixrude and Lithgow-Bertelloni[44].

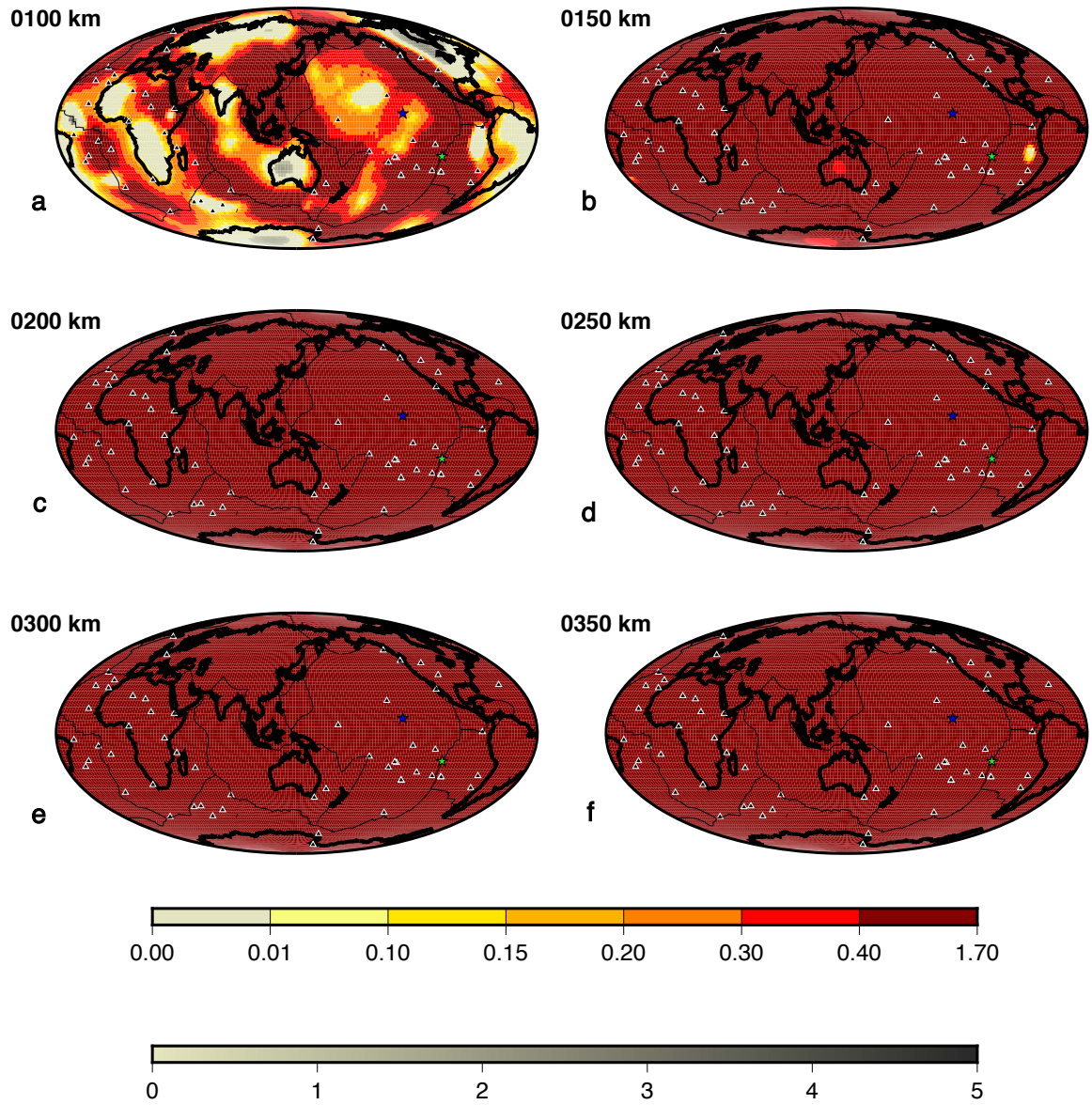

Fig. S8: Melt content at different depths in the upper mantle derived from the joint interpretation of QsADR17 and DR2020s, assuming a silica-deficient pyroxenite**.** The composition is taken from Table 1 of Stixrude and Lithgow-Bertelloni[44].

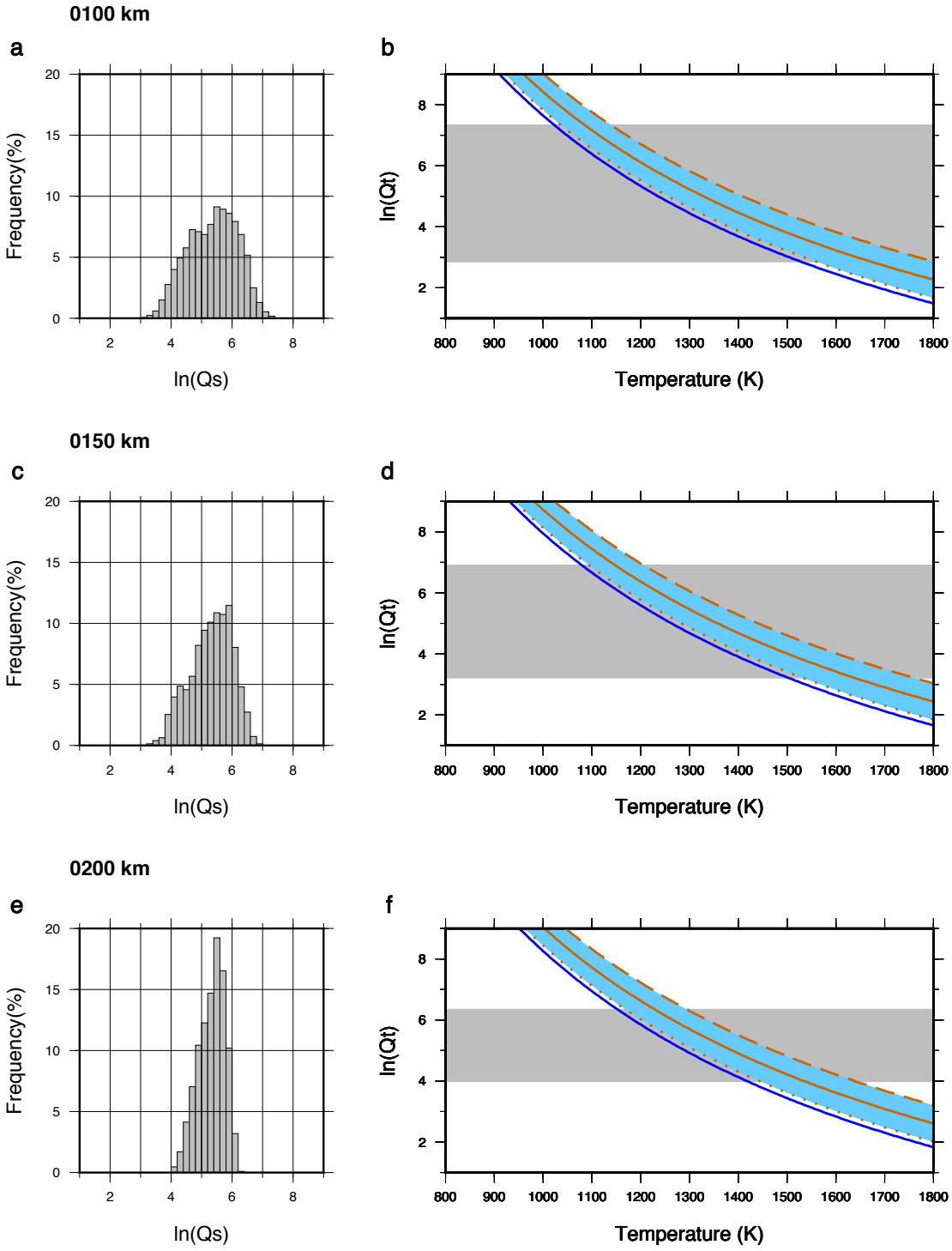

Fig. S9: Histograms of observed Qs and theoretical relations between Q and temperature according to Jackson et al.[13] at different depths in the upper mantle. Left column: Histograms of the distribution of $\ln(Q_s)$ values extracted at 100 (panel a), 150 (panel c) and 200 (panel e) km depth in QsADR17[30]. Right column: at the same depths, theoretical relation between $\ln(Q_t)$ and temperature computed using Eq. 1 for different grain sizes. The continuous lines in brown are the theoretical curves assuming a grain size of 10 mm. The light blue areas around this curve cover the influence of grain sizes from 1 mm (bottom dotted curve) to 100 mm (upper dashed curve). The dark blue curve is the theoretical curve for 125 ppm water computed using Eq. 5. The shaded grey area shows the range of Qs variations observed in QsADR17.

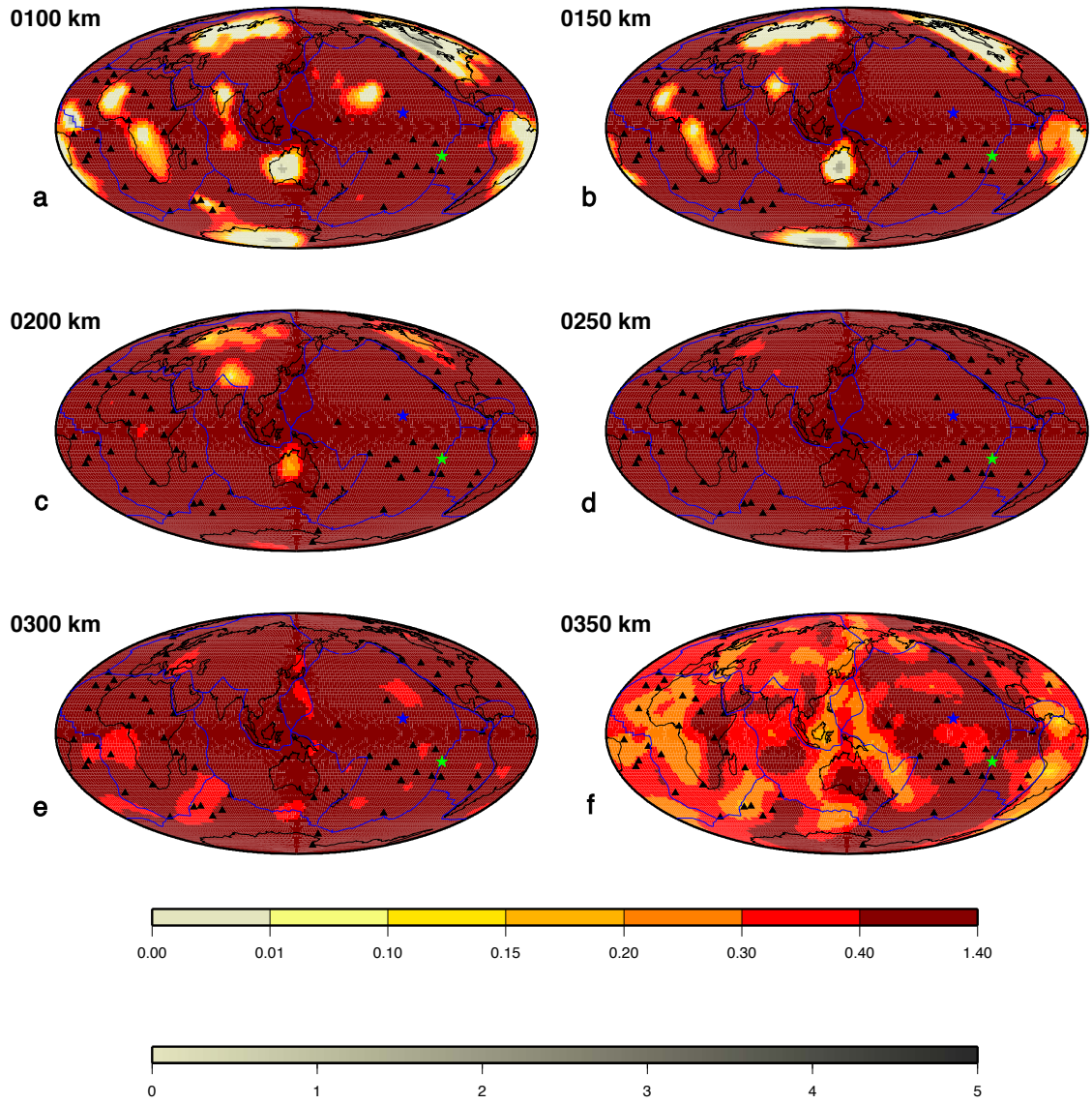

Fig. S10: Melt content at different depths using the anelasticity model of Jackson et al.[13] for a grain size of 10 mm and 125 ppm of water.

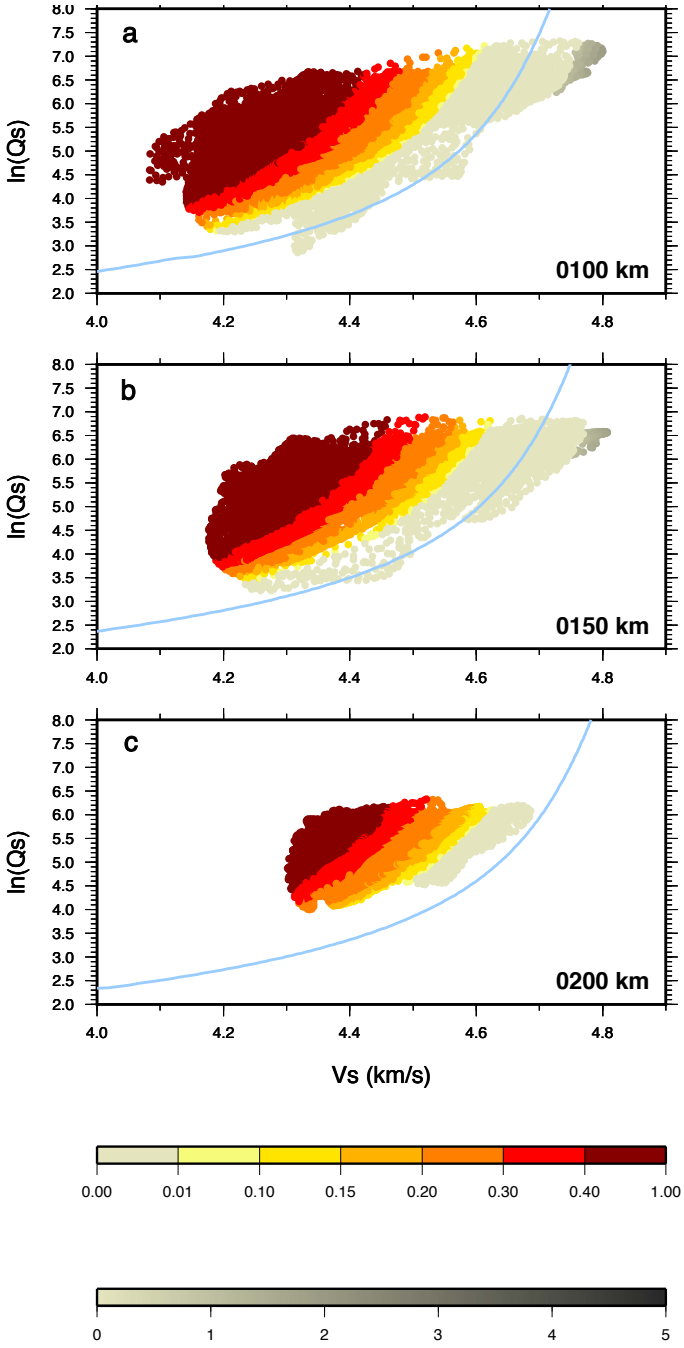

Fig. S11: Scatter plot showing shear attenuation as a function of shear velocity for the anelasticity model of Jackson et al.[13]. Same as Figure 2 but the colour scales indicate the departure from the anelasticity model of Jackson et al.[13] (light blue curve), for a grain size of 10 mm and a dry mantle.

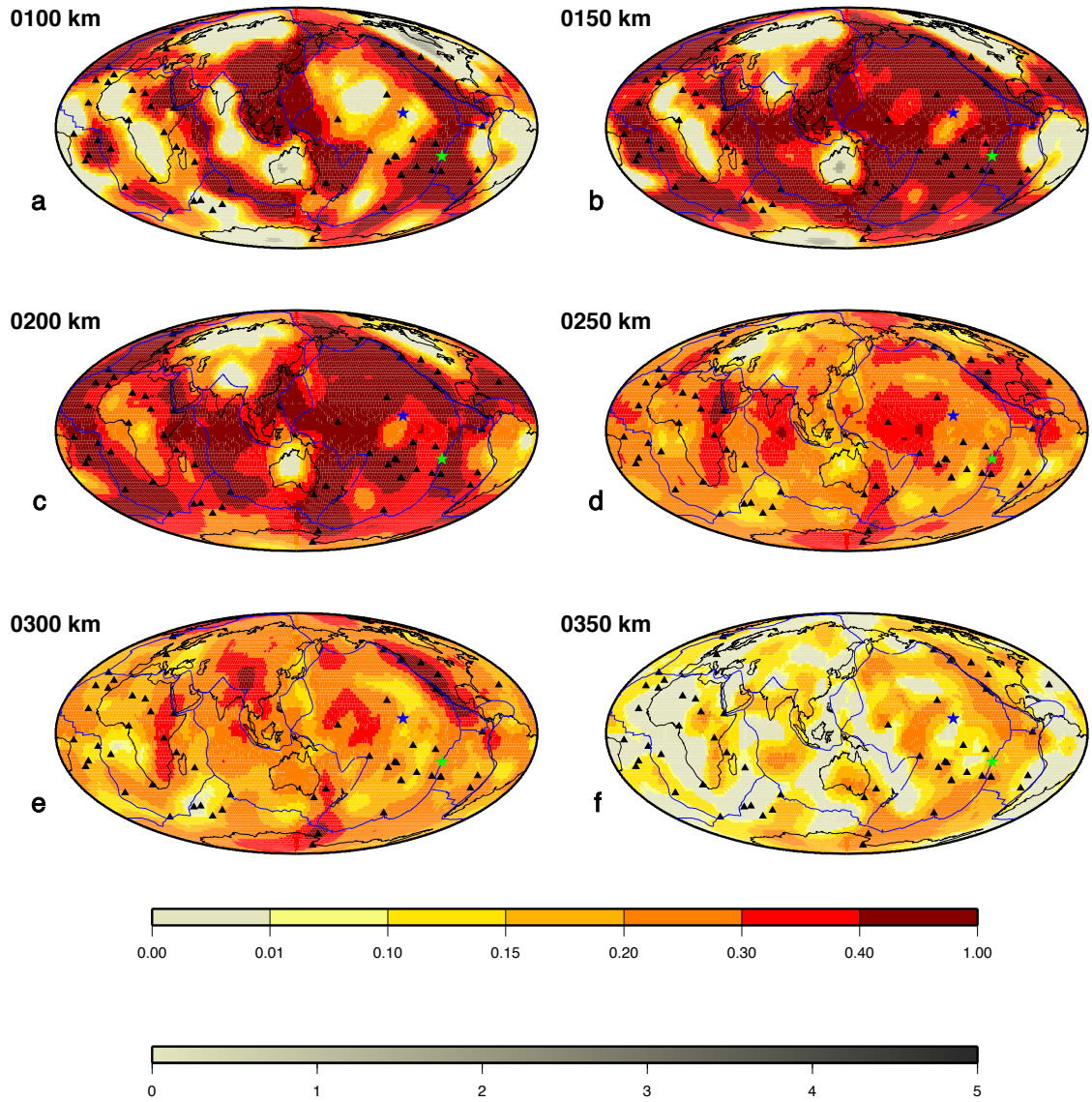

Fig. S12: Melt content at different depths for the anelasticity model of Jackson et al.[13]. Same as Figure 3 but colour scales indicate the departure from the anelasticity model of Jackson et al.[13], for a grain size of 10 mm and a dry mantle.

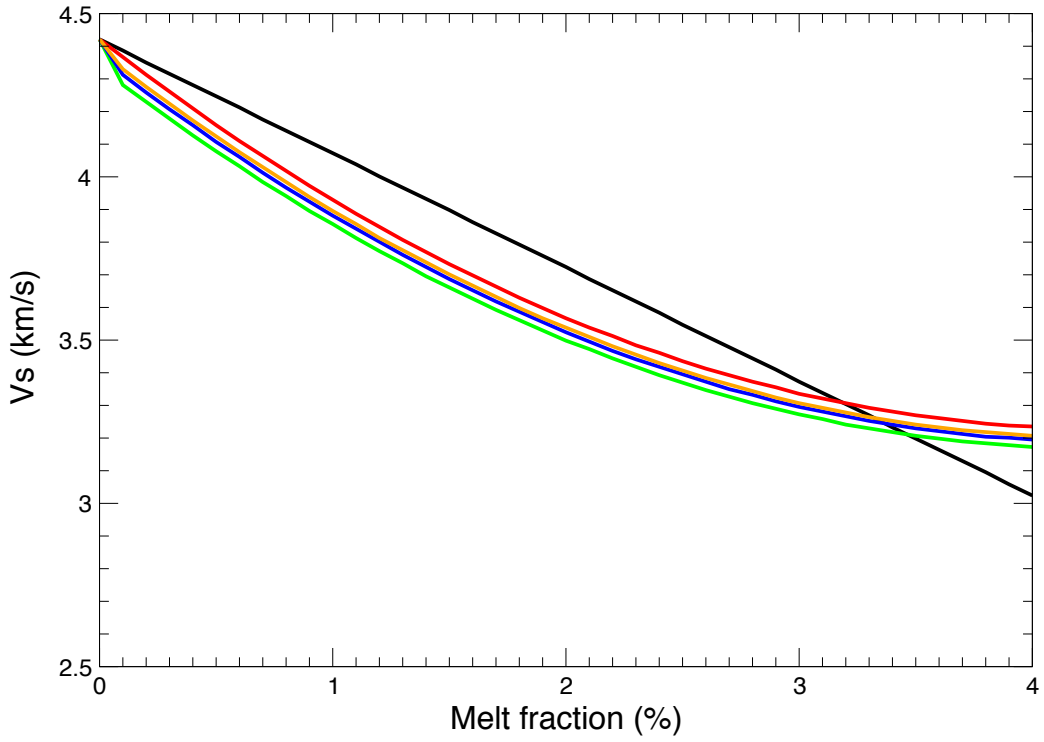

Fig. S13: Dependence of shear velocity on melt fraction φ. The linear Vs reduction of 7.9% per percent of melt[17] is shown in black from a reference velocity V_{ref} (set to 4.42 km/s). The polynomial expression used in this study ($V_s = 0.065\varphi^2 - 0.5565\varphi + V_{ref}$) is derived from experimental results[3] and is shown in red. The anelastic effect expected for seismic waves at high temperature[35] is shown assuming Qs=80, the value of PREM in the asthenosphere, for different values of α (green, blue and orange curves are for α=0.2, 0.3, 0.4) respectively. For small melt fractions (<1%), a stronger Vs reduction is obtained using the polynomial expression and the choice of α has a moderate effect.

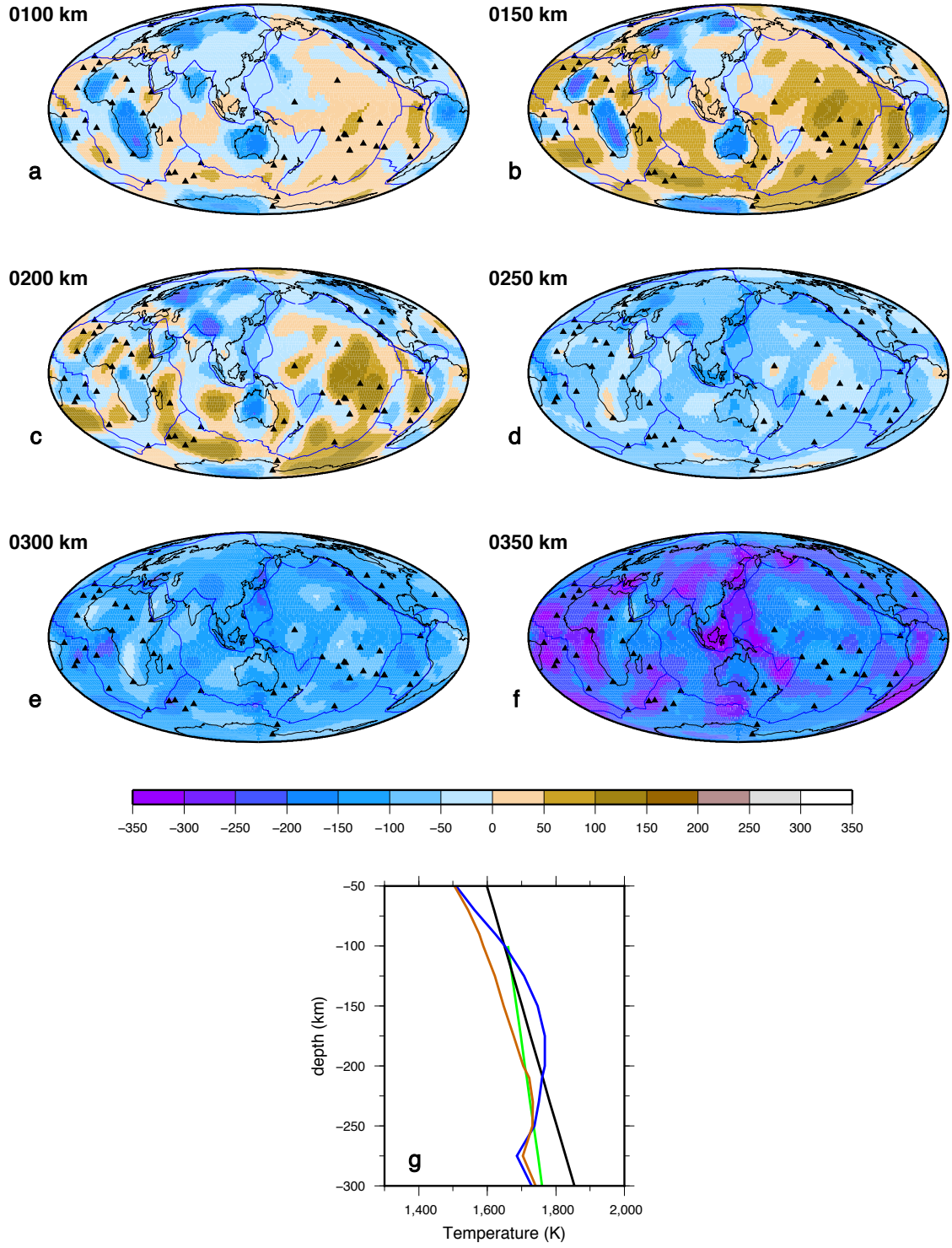

Fig. S14: Temperature predicted by our model (panels a-f) and compared with an oceanic solidus and a mantle adiabat (panel g). Panels a-f: Temperature anomalies maps in kelvins, with respect to an oceanic solidus[4] (black curve in panel g) at different depths in the upper mantle. Panel g: 1D temperature profiles averaged from these maps over oceanic (blue curve) and continental (brown curve) regions. These 1D profiles are compared with an oceanic solidus based on petrological observations[4] (black curve) and with a mantle adiabat[54] (green curve).

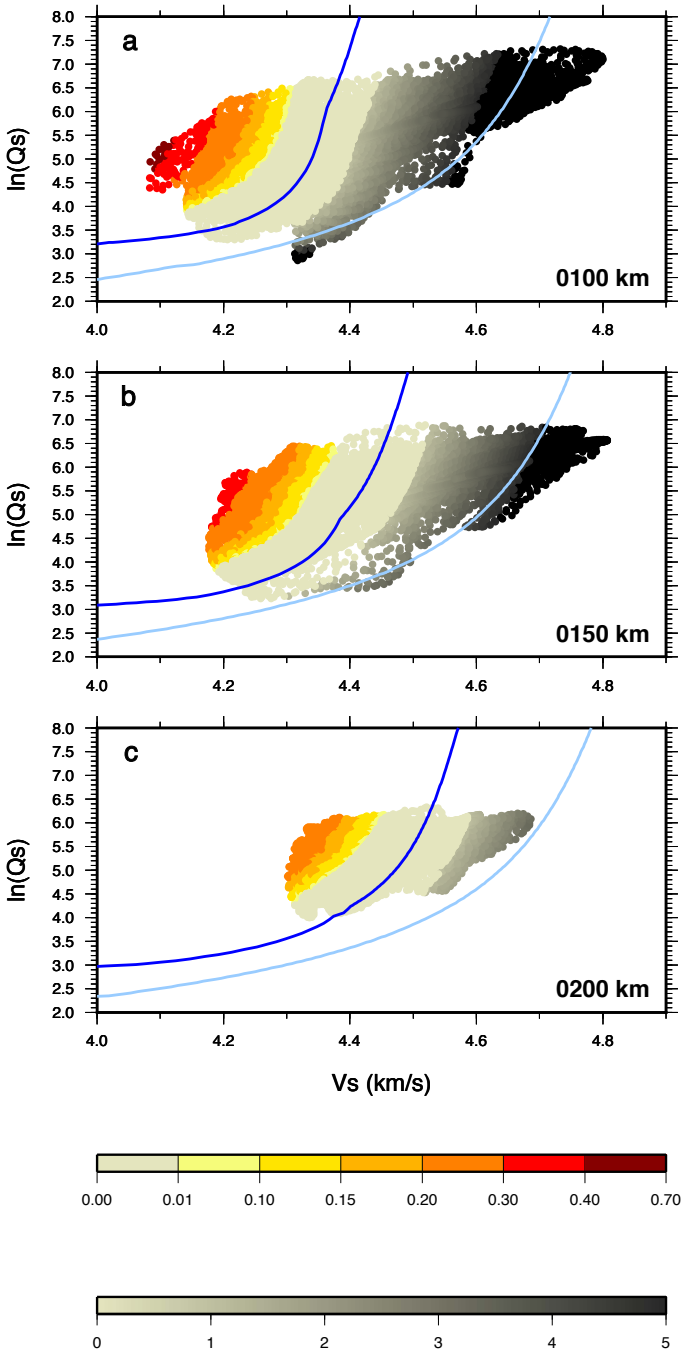

Fig. S15: Scatter plot showing shear attenuation as a function of shear velocity assuming a different shear modulus. Same as Figure 2 but the unrelaxed shear modulus μ_U needed to compute the temperature-dependent model (dark blue curve) is calculated using parameters proposed for the temperature model of the Pacific[4], instead of those deduced from Perple X[34] assuming a pyrolitic composition. The light blue curve is the theoretical prediction using the anelasticity model of Jackson et al.[13].

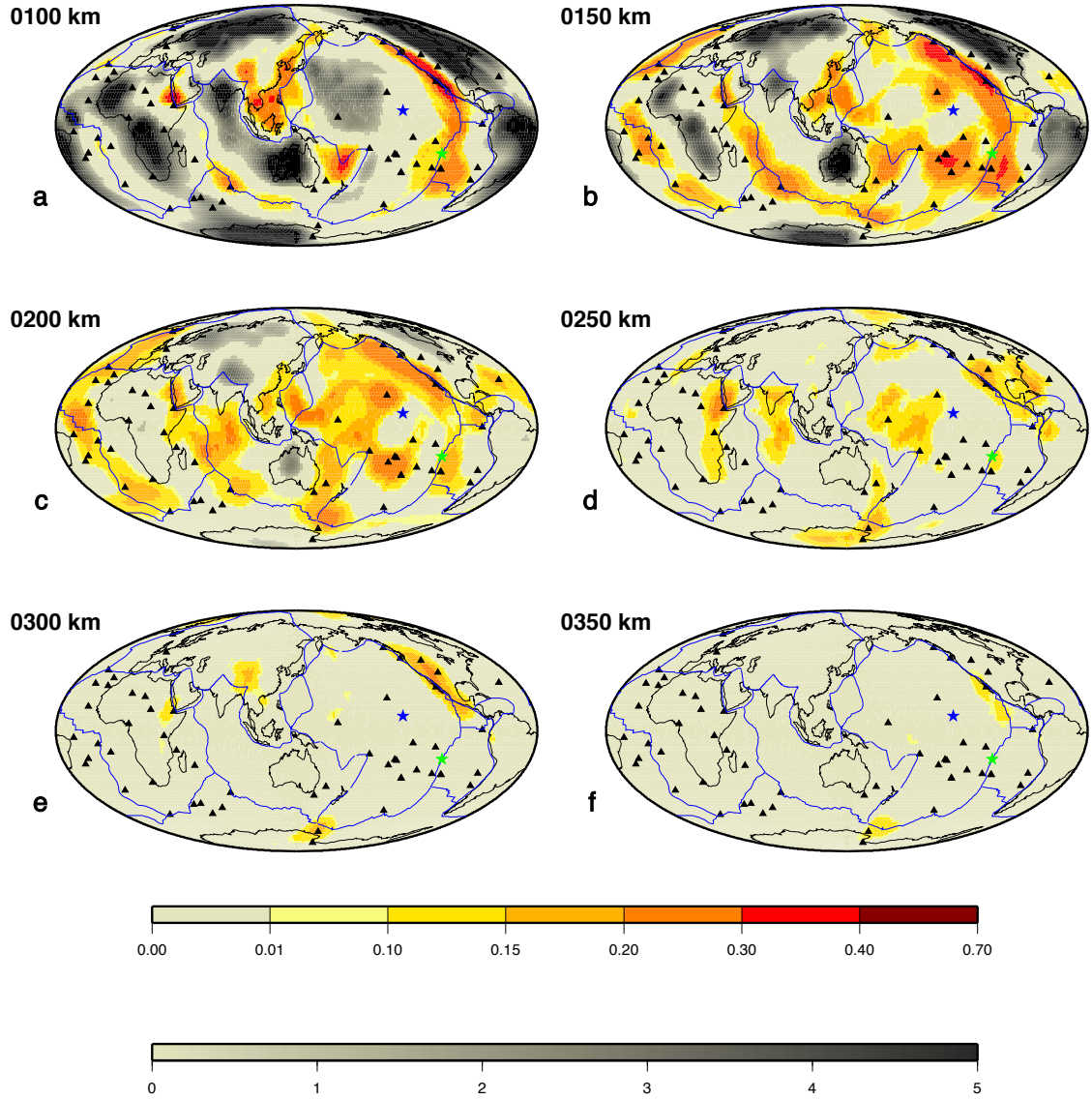

Fig. S16: Melt content at different depths for a different shear modulus. Same as Figure 3 but instead to estimate the unrelaxed shear modulus μ_U using Perple X[34] and a pyrolitic model, we use fitting parameters of the temperature model for the Pacific[4].

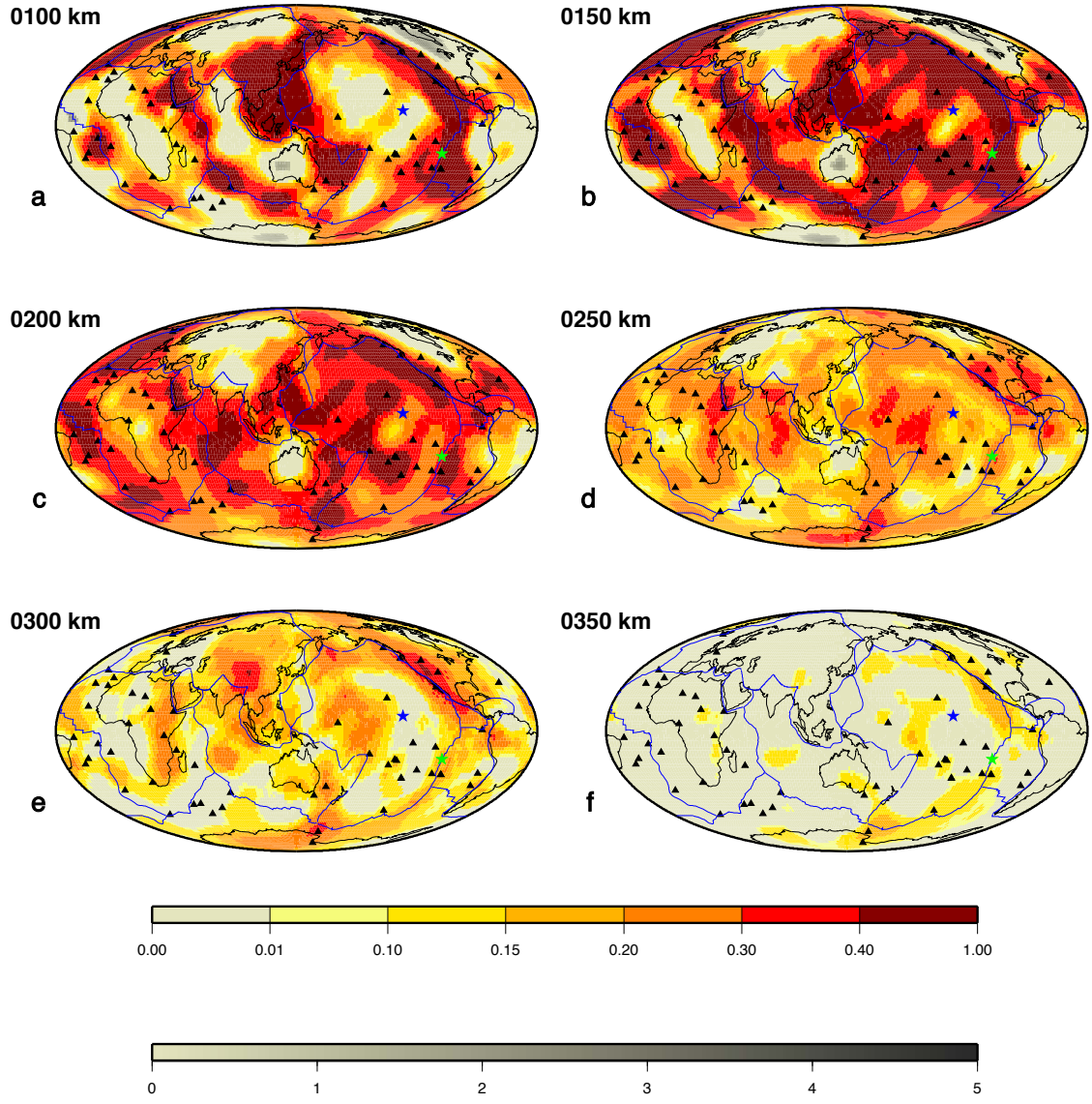

Fig. S17: Melt content at different depths for a different grain size. Same as Figure S12 but for a grain size of 100 mm.

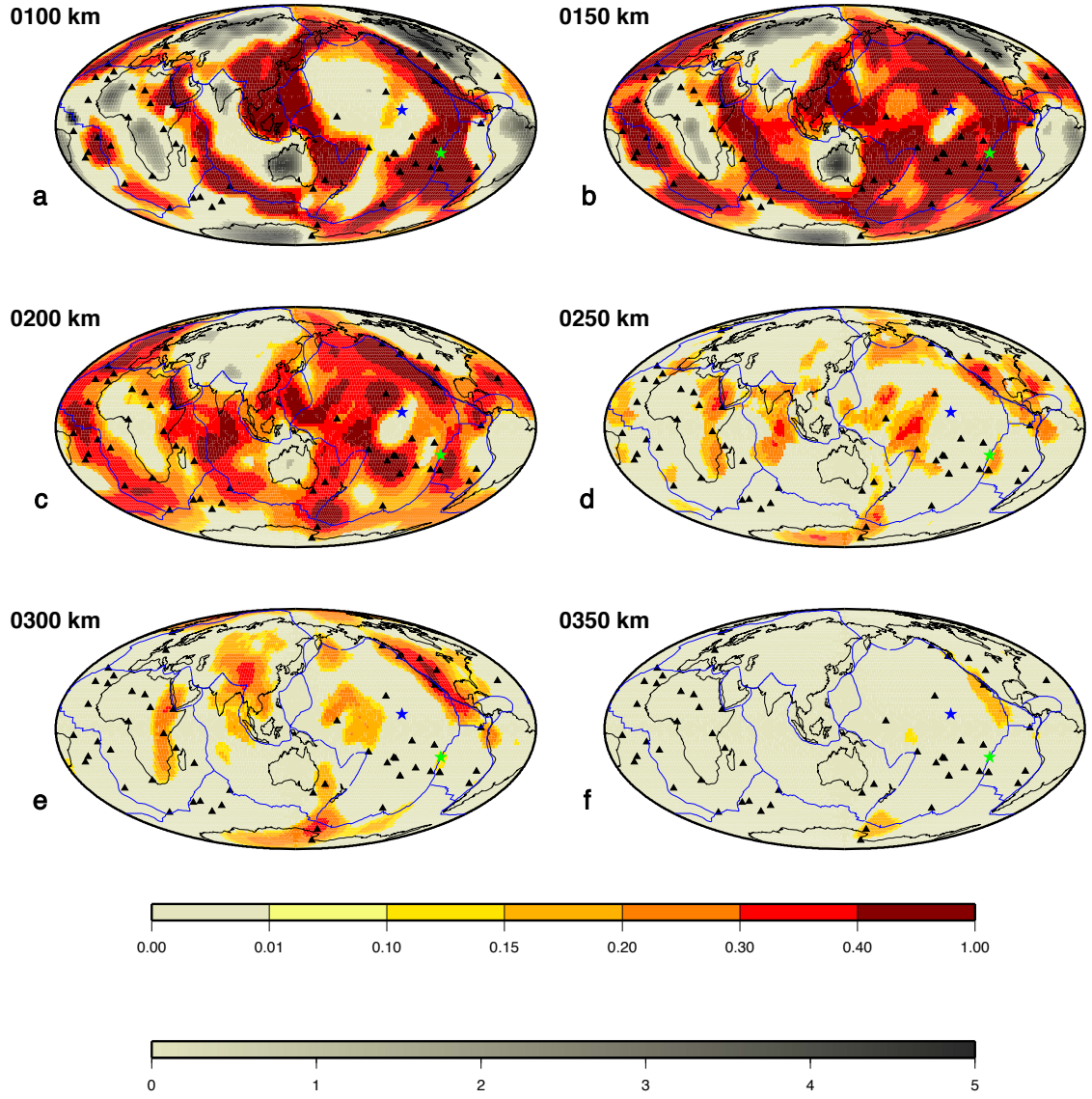

Fig. S18: Melt content at different depths for a different sensitivity of Vs to melt content. Same as Figure 3 but using a linear 7.9% Vs reduction per percent of melt[17] instead of the polynomial expression derived from experimental results[3]. The upper colour scale is slightly modified to allow melt content up to 1% (the maximum value at 100 km depth).

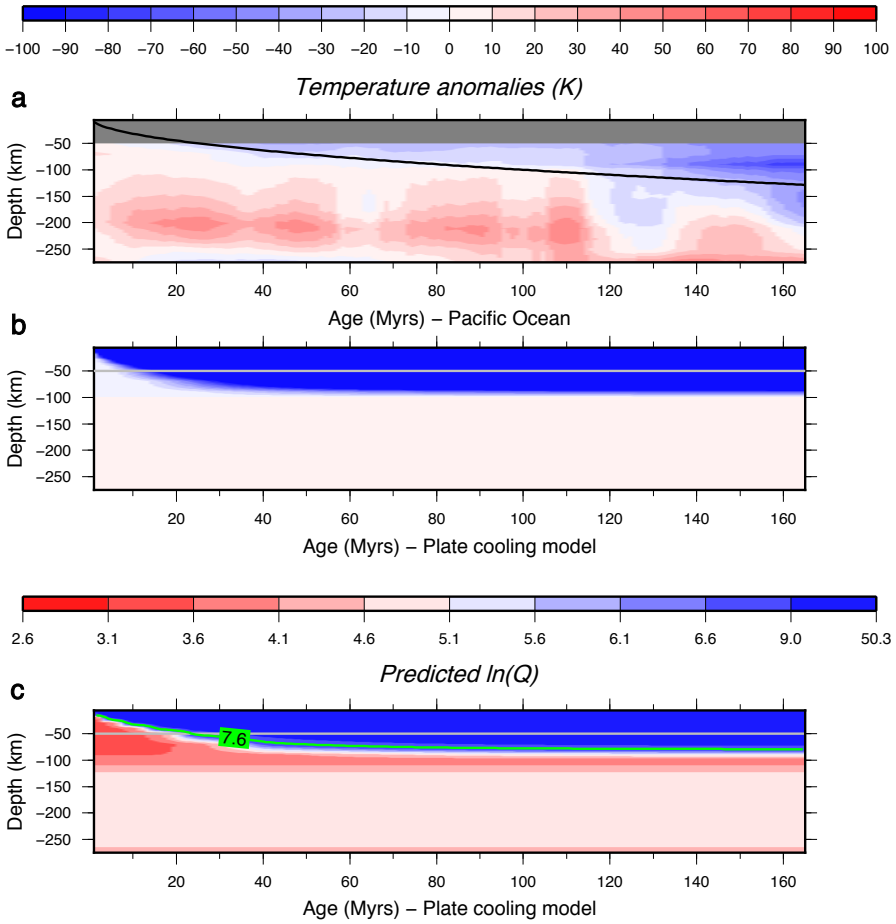

Fig. S19: Temperatures (panels a and b) and quality factor variations (panel c) as a function of sea-floor age. Temperature variations are shown with respect to the 1D profile of temperature at the ridge axis. Panel a: Temperature variations for the Pacific Ocean deduced from the interpretation of our Vs and Qs models using laboratory experiments[4]. Temperature is shown for depths larger than 50 km (we do not invert for the shallower attenuation that is not well resolved by long period surface waves). The continuous black line indicates the position of the thermal boundary layer for the half-space cooling model[52] (isotherm 1100°C). Panel b: Temperature anomalies predicted by a plate-cooling model[53]**.** Panel c: plate-cooling model converted into ln(Q) using experimental results[4] on thermal attenuation. The green line (ln(Q)=7.6 corresponding to Q=2000) is the limit above which surface waves cannot resolve accurately Q variations. In panels b and c, a horizontal grey line emphasizes the depth range (from 0 to 50 km) in which we have no attenuation observations.